

The Orbit of the Close Companion of Polaris: *Hubble Space Telescope* Imaging 2007 to 2014*

Nancy Ramage Evans¹, Margarita Karovska¹, Howard E. Bond^{2,3}, Gail H. Schaefer⁴,
Kailash C. Sahu³, Jennifer Mack³, Edmund P. Nelan³, Alexandre Gallenne⁵, and Evan D.
Tingle¹

Received _____; accepted _____

*Based on observations made with the NASA/ESA *Hubble Space Telescope*, obtained by the Space Telescope Science Institute. STScI is operated by the Association of Universities for Research in Astronomy, Inc., under NASA contract NAS5-26555.

¹Smithsonian Astrophysical Observatory, MS 4, 60 Garden St., Cambridge, MA 02138, USA; nevens@cfa.harvard.edu

²Department of Astronomy & Astrophysics, Pennsylvania State University, University Park, PA 16802, USA; heb11@psu.edu

³Space Telescope Science Institute, 3700 San Martin Drive, Baltimore, MD 21218, USA

⁴The CHARA Array of Georgia State University, Mount Wilson Observatory, Mount Wilson, CA 91023, USA

⁵European Southern Observatory, Alonso de Cordova 3107, Casilla 19001, Santiago, Chile

ABSTRACT

As part of a program to determine dynamical masses of Cepheids, we have imaged the nearest and brightest Cepheid, Polaris, with the *Hubble Space Telescope* Wide Field Planetary Camera 2 and Wide Field Camera 3. Observations were obtained at three epochs between 2007 and 2014. In these images, as in *HST* frames obtained in 2005 and 2006 which we discussed in a 2008 paper, we resolve the close companion Polaris Ab from the Cepheid Polaris Aa. Because of the small separation and large magnitude difference between Polaris Aa and Ab, we used PSF deconvolution techniques to carry out astrometry of the binary. Based on these new measurements, we have updated the elements for the 29.59 yr orbit. Adopting the distance to the system from the recent *Gaia* Data Release 2, we find a dynamical mass for the Cepheid of $3.45 \pm 0.75 M_{\odot}$, although this is preliminary, and will be improved by CHARA measurements covering periastron. As is the case for the recently determined dynamical mass for the Cepheid V1334 Cyg, the mass of Polaris is significantly lower than the “evolutionary mass” predicted by fitting to evolutionary tracks in the HR diagram. We discuss several questions and implications raised by these measurements, including the pulsation mode, which instability-strip crossing the stars are in, and possible complications such as rotation, mass loss, and binary mergers. The distant third star in the system, Polaris B, appears to be older than the Cepheid, based on isochrone fitting. This may indicate that the Cepheid Polaris is relatively old and is the result of a binary merger, rather than being a young single star.

Subject headings: stars: binaries; stars: variable: Cepheids; stars: massive; stars: masses

1. Introduction

The link between Cepheids and the extragalactic distance scale illustrates the importance of a thorough understanding of Cepheid physics. In addition to their significance as standard candles, they are benchmarks for confronting stellar-evolution theory. They ultimately become white dwarfs, which means a subset will be compact objects in binary/multiple systems, a part of a population from which exotic objects are formed (novae, supernovae, X-ray binaries). The long-standing “Cepheid mass problem” (the mass predictions from evolutionary tracks are larger than predictions from pulsation calculations) has been reduced through revision of interior opacities (e.g., Bono et al. 2001), but still persists. Measured dynamical masses for Cepheids, coupled with a well-determined luminosity, are needed to confront these questions as well as to provide predictions about the origin of late-stage exotic objects.

Polaris (α Ursae Minoris) is the nearest and brightest Cepheid. It is a member of a triple system, with its resolved 8th-mag F3 V physical companion, Polaris B, lying at a separation of $18''$. The Cepheid itself has been known for many years to be a single-lined spectroscopic binary with a period of about 30 years (Roemer 1965; Kamper 1996, hereafter K96, and references therein), whose components we denote Polaris Aa and Ab. Thus Polaris offers an opportunity for direct determination of a Cepheid’s dynamical mass. To date, V1334 Cyg is the only other Cepheid with a measured purely dynamical mass (Gallenne et al. 2013; 2018) in the Milky Way; however interferometric studies which resolve orbits will increase the number over the next few years (Gallenne et al. 2015). Cepheids in eclipsing binaries in the Large Magellanic Cloud summarized by Pilecki et al. (2018) provide an important comparison.

Recent papers have disagreed about the distance of the Polaris system. The *Hipparcos* mission (van Leeuwen 2007, hereafter vL07) measured an absolute parallax of 7.54 ± 0.11 mas

($d = 132.6 \pm 1.9$ pc). However, Turner et al. (2013, hereafter T13, and references therein) gave astrophysical arguments that the parallax of Polaris must be considerably larger, 10.10 ± 0.20 mas ($d = 99 \pm 2$ pc), but this was disputed by van Leeuwen (2013). More recently, Bond et al. (2018, hereafter B18) measured a parallax of only 6.26 ± 0.24 mas ($d = 160 \pm 6$ pc), using the Fine Guidance Sensors (FGS) on the *Hubble Space Telescope* (*HST*). Since Polaris itself is too bright for FGS measurements, B18 determined the parallax of the wide physical companion, Polaris B. The large distance based upon the FGS parallax implies a relatively high luminosity, indicating that Polaris pulsates in the second overtone rather than the fundamental mode. For the *Hipparcos* parallax, the pulsation is likely to be at the first overtone (e.g., Feast & Catchpole 1997; Bono et al. 2001; van Leeuwen et al. 2007; Neilson 2014). For the large parallax advocated by T13, the pulsation would be in the fundamental mode, as they argued.

In the recent Data Release 2 (DR2), the *Gaia* mission derived a parallax of 7.292 ± 0.028 mas for Polaris B (Gaia Collaboration et al. 2016, 2018a, 2018b). Polaris itself is too bright to have been measured for DR2. This result corresponds to a distance of 137.2 pc with a range of 136.61 to 137.67 pc. Applying the correction found by Lindegren et al. (2018) of +0.03 mas to the parallax reduces the distance to 136.6 pc. Polaris B has a magnitude $V = 8.65$, well below the brightness limit for *Gaia*. The discussion by Riess et al. (2018) of Cepheids finds a slightly larger zeropoint offset (-0.046 mas) for the Cepheids they discuss, although Polaris B is somewhat hotter (F3 V) and the zeropoint may have color dependence. Further discussion is given in Section 3.

Polaris is very unusual among Cepheids, in that its pulsation amplitude decreased over much of the 20th century. However, in recent years the amplitude has begun to increase again (e.g., Bruntt et al. 2008). This may indicate a very long-period pulsation/interference cycle.

Our team obtained near-ultraviolet images of Polaris with the High-Resolution Channel (HRC) of the Advanced Camera for Surveys (ACS) onboard *HST* in 2005 and 2006. These images succeeded in resolving the Polaris Aa and Ab pair for the first time, at a magnitude difference of 5.4 mag and a separation of about $0''.17$ (Evans et al. 2008, hereafter E08). This allowed us to estimate the first purely dynamical mass for any Cepheid (albeit with a large uncertainty). Since then, we have used *HST* cameras to make three more observations, which now cover a larger portion of the orbit. However, the new measurements were considerably more difficult and inexact, because the separation between Polaris and its close companion has been decreasing, and because the HRC was no longer available. In this paper, we report these new measurements, and update the dynamical-mass estimates.

2. Observations, Image Processing, and Deconvolution

Table 1 lists information about our three new *HST* observations, along with the previous 2005 and 2006 measurements given by E08. The new *HST* observations reported here were made in 2007, 2009, and 2014. In this section we give details of our observing strategy, the creation of combined images at each epoch, and finally the deconvolution of the images and astrometry of the binary.

2.1. Observing Strategies

Two different *HST* cameras were used for our new observations, as follows:

(1) *WFPC2 2007*. Following the successful detection by E08 of the close companion of Polaris with ACS/HRC in 2005 and 2006, we had planned to obtain an additional HRC observation in 2007. Unfortunately, the ACS suffered a failure in 2007 January, making it unavailable. We used instead the Wide Field Planetary Camera 2 (WFPC2), and the

observations were made on 2007 July 17. We chose the near-ultraviolet broad-band F218W filter, both because Polaris Ab is slightly hotter than the Cepheid, and because of the smaller point-spread function (PSF) at shorter wavelengths. We used a similar observing strategy as for the HRC observations, placing the target in the Planetary Camera (PC) CCD. The PC plate scale is $0''.046 \text{ pixel}^{-1}$, as compared with the ACS/HRC scale of $0''.026 \text{ pixel}^{-1}$. We first obtained a series of eight short (0.8 s) exposures spread over a three-point dither pattern. The telescope orientation was specified such that Polaris A and B would lie parallel to the edge of the PC field and symmetrically placed relative to the corners, and we positioned these targets close to the edge so as to minimize charge-transfer-inefficiency effects. This orientation also placed the location of Ab away from the diffraction spikes of Aa, for its anticipated position angle (P.A.). We then moved the telescope to put the wide companion Polaris B at the same position used for A, and obtained six longer exposures (50 s) in the same dither pattern. This provided a PSF standard at the same field position as Polaris A, exposed to about the same count level.

(2) *WFC3 2009*. The WFPC2 camera was removed from *HST* during the 2009 May Servicing Mission 4, and replaced with the Wide Field Camera 3 (WFC3). We observed Polaris with the WFC3 UVIS channel on 2009 November 18. The UVIS plate scale is $0''.040 \text{ pixel}^{-1}$. Because of the increased sensitivity of WFC3 relative to WFPC2, we used the narrow-band near-ultraviolet filter FQ232N, in order to avoid saturating the image of Polaris Aa. We again chose a telescope orientation to place Ab between the diffraction spikes of Aa. We obtained a total of nine dithered exposures of 0.5 and 0.7 s, with Polaris A placed near the center of a 2048×2048 -pixel subarray ($81'' \times 81''$). Then we placed Polaris B near the center of the field, and obtained five dithered exposures of 45 s each to use as a PSF reference.

(3) *WFC3 2014*. By the time of our final *HST* observations of Polaris, it had become

known that short exposures with WFC3 are affected by vibrations in the camera due to the shutter mechanism (“shutter jitter”; see Sahu et al. 2014 for a technical discussion). Exposures with the shutter in the “A” blade position are less affected than those in the “B” position, so we used the newly available `BLADE=A` option for all of our exposures. Instead of using longer exposures on Polaris B as a PSF reference star, which would be much less affected by shutter jitter, we observed γ Cygni—a star with nearly the same magnitude, color, and spectral type as the Cepheid—immediately after the Polaris observation. We obtained 14 dithered FQ232N exposures on Polaris of 1.5 s each (which the 2009 exposures indicated would not be saturated), and chose a telescope orientation that placed Polaris Ab at an optimum location in the PSF to avoid diffraction spikes and filter ghosts, based on our analysis of the 2009 images. This was followed by a set of 12 essentially identical dithered exposures on γ Cyg. The observations were otherwise very similar to those made in 2009.

Our first attempt at these observations (2014 March 17) suffered a loss of guide-star lock partway through the γ Cyg visit, so that we did not have useful PSF images. These data were not included in our data analysis. Both sets of observations were repeated successfully on 2014 June 26.

2.2. Combining the Dithered Images

As described above, we obtained a set of dithered exposures of Polaris A and B at two epochs, and of Polaris A and γ Cyg at a single epoch. In order to combine these images into optimal single images at each epoch, we used the `AstroDrizzle` package developed at the Space Telescope Science Institute (STScI), running under `PyRAF`¹. The resulting combined

¹`AstroDrizzle` and `PyRAF` are products of the Space Telescope Science Institute, which is operated by AURA for NASA.

images have a pixel scale of $0''.02$. For the WFC3 data in 2009 the problem of “shutter jitter” was a concern. We experimented with the images, and found that the “even” images in the dither pattern were better quality, and were able to test the effect on the location of the companion.

2.3. Deconvolution and Astrometry of Polaris Ab

The observed stellar images are blurred by the PSF of the telescope and camera optics, and the finite size of the detector pixels. To remove the effects of this blurring we have in principle several options, including a subtraction of the PSF (based on images of a reference point source), fitting of a model for the source plus PSF to the observed source, or a full deconvolution of the PSF.

Because of the small separation, the large magnitude difference between the Cepheid Polaris Aa and its companion Polaris Ab, and the larger plate scales compared to the ACS/HRC used in our earlier observations, we could not use direct PSF model fitting for any of the more recent observations. Direct PSF subtraction was also unable to detect the companion. Therefore, we applied deconvolution/restoration techniques, using the observed single point-like reference stars as models of the PSF.

We applied two image-restoration methods. One of them is the well-known Richardson-Lucy (R-L) deconvolution technique (Richardson 1972; Lucy 1974), and the other is a statistical deconvolution (restoration) technique called EMC2 (Expectation through Markov Chain Monte Carlo). The EMC2 technique uses a wavelet-like multiscale representation of the true image in order to achieve smoothing at all scales of resolution simultaneously (see Esch et al. 2004; Karovska et al. 2005, 2010).

As described above, for the 2007 and 2009 observations we used Polaris B as a PSF

reference star, which we had placed at the same field location as Polaris A. For these two epochs, the R-L technique successfully resolved the companion. Figures 1 and 2 depict the results of the deconvolutions, with the locations of the companion Polaris Ab marked with circles, connected by arrows to the center of Polaris Aa. The last two columns in Table 1 give the derived P.A. and separation of Polaris Ab. The quoted errors estimated by eye correspond to one pixel in the drizzled image ($0''.02$). This is conservative for the 2009 WFC3 observation, where they may be smaller.

By the time of the 2014 observation, Polaris Ab had moved much closer to Polaris Aa, making it considerably more difficult to separate the two components. We did, however, have images of the PSF reference star γ Cyg, obtained with the same exposure times as Polaris, and thus affected by the same amount of shutter jitter. For this observation, we applied the EMC2 deconvolution technique, which is better suited for detecting faint companions.

Given the small separation and large magnitude difference, we had to search for Polaris Ab amidst the PSF structure and noisy remnants of the deconvolution. However, our search was guided by a predicted location of the companion, based on an existing orbital fit to the previous measurements. This facilitated the search for the companion, and we believe we have detected it.

In Figure 3 we show the deconvolved 2014 image. A circle marks the region where we believe we may have detected the companion. Also included are two smaller circles indicating the predicted locations. The first uses the orbit from the spectroscopic orbit, our *HST* observations from 2005 to 2007, and the astrometric measurements from Wielen et al. (2000). The second uses a slightly modified orbit with 1σ change in the inclination. The resulting P.A. and separation are listed in the bottom row in Table 1. The quoted error corresponds to the drizzled pixel size of $0''.02$. Although the 2014 detection is not as

clear as in the earlier observations, it may provide an additional constraint on the orbit. Unfortunately, for the remaining lifetime of *HST*, the separation will be too close to be resolved.

3. Visual Orbit for Polaris Aa–Ab

Our additional *HST* measurements of Polaris Aa–Ab substantially improve the orbital coverage, compared with the results presented by E08. We have fitted new orbits to the five astrometric data points presented in Table 1, and also to a subset of only the first four points, using a Newton-Raphson method to minimize χ^2 by calculating a first-order Taylor expansion for the equations of orbital motion. Since we have only four or five astrometric observations, covering only a small portion of the orbit, we fixed the values of the spectroscopic parameters of the orbital period P , eccentricity e , and longitude of periastron passage ω , to those determined by K96. The date of periastron passage T_0 reported by K96 was discussed and updated by Wielen et al. (2000), and we adopt their value. We then solved for the remaining parameters of the angular semi-major axis a , orbital inclination i , and the position angle of the line of nodes Ω . We obtained formal errors for each of the free parameters from the diagonal elements of the covariance matrix. To account for the uncertainties in the spectroscopic orbital parameters, we computed a series of 10,000 orbital solutions where we randomly varied P , T_0 , e , and ω within their 3σ uncertainties, and solved for the best-fit values of a , i , and Ω for each iteration. We computed the standard deviation for each parameter’s distribution, and added these uncertainties in quadrature to the formal errors computed from the best-fit solution when fixing the spectroscopic parameters.

We present two orbital solutions. One uses all of the *HST* data, and the other omits the 2014 measurement, which is the most uncertain. The final orbital parameters and

uncertainties are presented in Table 2 for both solutions.

In Figure 4 we show the *HST* measurements compared with the best-fit orbit for all data. The shared gray area shows the range of orbital solutions that fit the data. This region was computed using two different methods. As described above, in the first method we randomly varied the spectroscopic parameters within their 1σ uncertainties, and re-derived the best-fitting orbit for each iteration. In the second method, we fixed the spectroscopic parameters and randomly varied a , i , and Ω in order to search for orbital solutions within $\Delta\chi^2 = 3.53$ of the minimum, corresponding to a 68.3% confidence interval, for the three free parameters. The shaded region in the figure represents the maximum deviations in orbital solutions obtained from these two samples. The residuals in separation and P.A. compared with the best-fit orbit are plotted in Figure 5.

By assuming a parallax π for the system, we can then compute the total mass of Polaris Aa and Ab through Kepler’s Third Law: $M_{\text{tot}} = M_{\text{Aa}} + M_{\text{Ab}} = a^3/(\pi^3 P^2)$, where the masses are in solar units, a and π in seconds of arc, and P in years. Using the radial-velocity amplitude of Polaris Aa ($K_{\text{Aa}} = 3.72 \pm 0.03 \text{ km s}^{-1}$) from the spectroscopic orbit of K96, we can derive individual masses of Aa and Ab. We show the resulting dynamical masses using both the *Gaia* parallax and the *Hipparcos* parallax in Table 3. We note that the errors for the distance from *Gaia* are small, but the mass itself depends on the orbital solution, which will become better defined during the periastron passage. The comparison in Table 2 of the orbit omitting the least accurate point illustrates the possible difference in the solutions.

The mass derived depends heavily on the parallax. The parallax from *Gaia* DR2 for Polaris B has reasonable “excess noise” of 0.0 and a reduced χ^2 of 2.7. The “goodness of fit” is 12.2, which is higher than the desirable 9, but within a reasonable range. The use of a zero point correction to *Gaia* parallaxes adds to the uncertainty. The mass of the Cepheid without the correction becomes $3.50 \pm 0.76 M_{\odot}$. We anticipate improvement in the

mass determination from subsequent *Gaia* releases such as DR3, as well as more complete observations of the orbit.

We note two further points about the adopted parallax for the Polaris system.

(1) Using the T13 parallax would result in a mass for the Cepheid of only $1.08 M_{\odot}$, far smaller than either the observational or theoretical predictions for a Cepheid. We believe the large parallax advocated by T13 is now definitively ruled out. (2) We recomputed the FGS parallax reported by B18, by adopting as input values the parallaxes and proper motions for the background reference stars as given in the *Gaia* DR2. This actually makes the derived parallax of Polaris B even smaller than given by B18. At this point, given the good agreement between the *Hipparcos* parallax for Polaris A and the DR2 parallax for Polaris B, we no longer advocate the FGS parallax. We are examining reasons why it might be incorrect (such as the possibility that Polaris B could be a marginally resolved close binary).

Table 3 also lists, in the bottom line, the mean visual absolute magnitude of the Cepheid Polaris Aa, calculated by assuming a mean apparent magnitude of $\langle V \rangle = 1.982$ and a reddening of $E(B - V) = 0.01 \pm 0.01$ (see B18 and references therein), and adopting the two different parallaxes.

4. Discussion

4.1. Properties

Based on the updated results given in this paper (which still covers only a fraction of the entire 29.95 yr orbit), we now compare the masses in Table 3 with expectations from current Cepheid calibrations. For the Cepheid, Polaris Aa, the mass prediction is compared below with the measured mass of the Cepheid V1334 Cyg (Gallenne et al. 2018) as well

as with evolutionary tracks. There is also information about the astrometric companion, Polaris Ab, which was resolved by the *HST* HRC of the ACS at an epoch when the separation was wider. In E08, its mass was estimated based on photometric measurements to be $1.3 M_{\odot}$. This is in reasonable agreement with the estimate from the orbit (Table 3) but more precise masses for the Cepheid and the companion await more complete coverage of the orbit. The properties of both the Ab and B components of the system are discussed further compared with an isochrone in the discussion of mergers below.

4.2. Questions and Implications

As the nearest Cepheid, Polaris has measured properties which are available for only a few other Cepheids which provide a number of distinctive clues and raise questions which may be answered as the orbit becomes better defined. In this section we discuss recent results in several areas relevant to the interpretation of a measurement of the mass (and luminosity) of Polaris. The most important comparison with the preliminary mass of Polaris is with the recently determined mass of V1334 Cyg, and a comparison of these two stars with evolutionary tracks. Subsequently we discuss the period change (often interpreted as a direct measure of evolution), instability strip crossing, possible mass loss or a previous merger, and implications from abundances.

4.2.1. Pulsation Mode

Fig. 6 shows the location of Polaris in the Leavitt period-luminosity relation, using the *Gaia* absolute magnitude M_V . The comparison Cepheids have FGS trigonometric parallaxes (Benedict et al. 2007), *HST* spatial-scan parallaxes (Riess et al. 2018b), and the light-echo distance of RS Pup (Kervella et al. 2014). $\langle V \rangle$ and $E(B - V)$ have been taken

from the Galactic Cepheid Database (Fernie et al. 1995). While *Gaia* results for a large Cepheid sample will undoubtedly contribute immensely to the Leavitt Law, the brightest Cepheids are challenging for *Gaia*, so we use the previous *HST* results for this figure. The result from *Gaia* for Polaris B and hence the Cepheid Polaris Aa is consistent with pulsation in the first-overtone mode (though second overtone is still within the errors). We will treat the Cepheid as a first-overtone pulsator below.

4.2.2. Comparison with V1334 Cyg

V1334 Cyg is another overtone pulsator with a similar (fundamentalized) period (4.74^d) and luminosity to Polaris. Its mass and distance have been measured by Gallenne et al. (2018) to unprecedented accuracy using interferometry combined with radial velocities from the visible and ultraviolet, based on the orbit of Evans (2000). They find a Cepheid mass of $4.288 \pm 0.133 M_{\odot}$ and a distance of 720.35 ± 7.84 pc, corresponding to an absolute magnitude $M_V = -3.37$ (including a correction for the companion), which probably provides the best estimate of the expectation for Polaris. Polaris has a somewhat longer period than V1334 Cyg and a slightly brighter $M_V = -3.73 \pm 0.03$. The mass of the Cepheid Aa (*Gaia*; Table 3) is smaller ($3.45 \pm 0.75 M_{\odot}$), but the mass will not be final until the orbit is more fully covered. The mass of Polaris Aa only differs by a little more than 1σ from that of V1334 Cyg and the luminosities are similar. We discuss the rapid period change and variation in pulsation amplitude of Polaris below but we draw attention to the fact that V1334 Cyg shows no indication of period change, at least since 1968 (Berdnikov et al. 1997). In the previous discussion (B18), when Polaris appeared to be a second-overtone pulsator, it seemed likely that the different pulsation mode might be responsible for the difference in the envelope pulsation properties (period change and amplitude variation). However it now seems most likely that both stars are pulsating in the same mode, illustrating a range of

envelope pulsation properties.

4.2.3. Evolutionary Tracks

The combination of observed mass and luminosity is needed for comparison with evolutionary tracks. For a number of years it has been clear that a moderate amount of core convective overshoot in intermediate-mass main-sequence stars increases the fuel available and ultimately the luminosity of the “blue loops”, the stage at which Cepheids are found. (See Nielson et al. 2012 for examples of this effect.) This has the unfortunate counter effect of decreasing the temperature range of the blue loops so that typically evolutionary tracks for stars less massive than $5 M_{\odot}$ do not penetrate the instability strip (e.g., Fig. 2 in Neilson et al. 2012a). Recently an additional parameter has been explored in detail: rotational velocity. Anderson et al. (2014) provide evolutionary tracks for a range of initial rotations, which produce results similar to convective overshoot calculations: more luminous blue loops for a given mass. However, there is less suppression of loops for lower mass stars. Either of these possibilities or a combination may ultimately prove to be an accurate description, and the blue loops are notoriously sensitive to input parameters. However, at present it is not clear whether either theoretical approach matches the masses available or those expected in the near future.

In Fig. 7 we show the comparison between the evolutionary tracks with rotation discussed in Anderson et al. (2014) which are taken from Georgy et al. (2013). Polaris and V1334 Cyg have luminosities from *Gaia* (Table 3) and Gallenne et al. (2018) respectively. Temperatures are from $(B - V)_0$ (Evans 1988 and Evans et al. 2013 respectively) and the temperature color calibration as discussed in Evans & Teays (1996). However, masses inferred from the luminosities of the evolutionary tracks in Fig. 7 are about $5 M_{\odot}$, which is larger than the measured values, even for V1334 Cyg. This is true even when the stars start

their main-sequence life with a large rotational velocity. The mass of Polaris estimated using the evolutionary tracks in Fig. 7 (the “evolutionary mass”) is approximately $5.5 M_{\odot}$ for the tracks incorporating maximum rotation, but $6.0 M_{\odot}$ without rotation. These values are discrepant by 2.7σ and 3.4σ from the measured mass of $3.45 \pm 0.75 M_{\odot}$ (Table 3). However, only a small portion of the visual orbit is currently covered; a systematic offset of 3σ in the semi-major axis as the periastron passage is mapped in future observations would bring the mass of Polaris in agreement with the evolutionary masses.

In Fig. 8 we compare several representative evolutionary tracks in the “blue loop” section of the HR diagram. Specifically, $5 M_{\odot}$ tracks are plotted from the Geneva series (Georgy et al. 2013), the MIST series (Choi et al. 2016) and the PARSEC set (from `\protect\protect\protect\edefOT1{OT1}\let\enc@update\relax\protect\edefcmr{cmr}\protect\` based on the results from the Bressan et al. (2012) group. We selected $5 M_{\odot}$ tracks because they cover the temperature range of the instability strip and are available for a range of rotational velocities from several codes. For all three codes, tracks are shown with zero initial rotation. For Geneva and MIST, a track with substantial initial rotation is also shown (0.95 critical breakup speed for Geneva, 0.4 critical velocity for MIST). Fig. 8 shows the resulting variation in luminosity from the different codes as well as differing predictions for the incorporation of main sequence rotation.

V1334 Cyg is the first Cepheid with a dynamically determined mass with a small enough uncertainty ($4.288 \pm 0.133 M_{\odot}$) to strongly constrain the tracks. The most important point in Fig. 8 is that V1334 Cyg is *significantly* more luminous than the predictions for its mass from the calculations regardless of the code or rotation. An alternate description is that the Geneva tracks in Fig. 7 indicate that its mass is approximately $5 M_{\odot}$, which is $0.7 M_{\odot}$ larger than the measured mass.

A further note about the mass of V1334 Cyg is that it strongly constrains the lower

mass at which a star destined to become a Cepheid can enter the instability region after the red giant branch. Current tracks in Fig. 7 show that a $4 M_{\odot}$ star would not become hot enough. This is doubly true in that overtone pulsators are found among shorter period stars (even when “fundamentalized”) on the blue side of the instability strip. Thus, a track has to become hot enough to reach the blue region of the Cepheid instability strip.

Another parameter which is directly comparable with the predictions of evolutionary tracks is the radius. Mérand et al. (2006) measured an angular diameter of Polaris of 3.123 ± 0.008 mas, which corresponds to $46 R_{\odot}$ using the *Gaia* distance. We can make an approximate comparison between this and the results of the evolutionary tracks (Anderson et al. 2016) using the luminosity and temperature tabulated in their Table A.4. In the comparison we use the Milky Way metallicity, an initial rotation which is half critical breakup rotation, a mass of $5 M_{\odot}$, and first-overtone pulsation. The $5 M_{\odot}$ evolutionary track does not cover the full temperature width of the instability strip for the second and third crossing (discussed below), but rather enters the cool edge and then turns in the middle and returns to the cool edge, being the lowest mass of the computed tracks to enter the instability strip. However, the truncated second and third crossings cover the range of radii of 42 to $52 R_{\odot}$ while the first crossing spans 26 to $33 R_{\odot}$. Thus, in this approximate comparison, the third crossing (increasing period) is in reasonable agreement with the measured radius.

4.2.4. *Period Change*

Polaris undoubtedly has a changing period (Neilson et al. 2012b and references therein). A changing period is typically interpreted as resulting from evolution through the instability strip; however there are a number of indications that more than this simple interpretation is needed. Overtone pulsators appear to have higher rates of period change

than fundamental-mode pulsators of comparable period (Szabados 1983; Evans et al. 2002). This would, in fact, explain what is described as the anomaly of large period changes in short-period Cepheids by Turner et al. (2006). Studies using spectacular satellite observations (*Kepler*, *CoRoT*, *MOST*, *WIRE*) are alerting us to hitherto unknown pulsation behavior: new modes and interactions. For instance, first-overtone Cepheids in the Small Magellanic Cloud have peculiarities which may be related to nonradial pulsation (Smolec & Sniegowska 2016). In addition, continuous sequences of high-quality photometry with the *MOST* satellite of RT Aur (fundamental mode) and SZ Tau (first overtone) confirm that overtone cycles are less stable than fundamental mode cycles (Evans et al. 2015), though this has been disputed by Poretti et al. (2015).

Thus, while Polaris’s rapid period change has sometimes been interpreted as indicating a first rather than a third crossing of the instability strip (Turner et al. 2005), the working model here is that for overtone pulsators, period changes are not *strictly* due to evolution through the instability strip. Rather period changes are at least partially due to some aspect of pulsation that we do not yet fully understand. Other characteristics of Polaris’s pulsation support this. While the period change O-C (observed minus computed) diagrams suggest a parabola, the actual form is more complex, with a “glitch” about 40 years ago (Turner et al. 2005; Neilson et al. 2012). This requires two tightly constrained parabolas to fit the data. Furthermore, the pulsation amplitude of Polaris has a marked drop followed by a gradual increase over many decades, a phenomenon shared by at most one or two other Cepheids (Bruntt et al. 2008; Spreckley & Stevens 2008). A variable amplitude (decreasing and increasing) is much more likely to be due to a pulsation interaction than to an evolutionary effect, which would be expected to go in one direction only. In fact the classical Cepheid with the most prominent amplitude variation is V473 Lyr, which is a second-overtone pulsator.

Neilson et al. (2012) have made a population synthesis analysis of period changes in Cepheids and conclude that both main sequence core convective overshoot and mass loss (see below) are needed to match the observations to the predictions. This is based both on the size of the period change and also the proportion of second crossing (period increase) to third crossing (period decrease) stars. However, the working model above is that many of the short period stars are overtone pulsators and hence the period changes are determined by a pulsation component as well as an evolutionary component. Neilson et al. draw attention to the fact that short-period stars fit the predictions less well than long-period stars. If the short-period stars omitted for this reason, Fig. 3 in Neilson et al. shows that for the long-period stars, the distribution of period changes is well matched by evolutionary predictions. It is likely that this also changes the proportion of positive to negative changes as well, but a firm statement requires the detailed identification of overtone pulsators. Note further, that the period changes discussed are biased in the sense that they include only stars with measurable period changes. A large fraction of Cepheids in the Szabados catalogs (1977, 1980, 1981, 1989, 1991) show no period change, at least over the 60 years for which we have photometric observations. Presumably their periods also change as they evolve, but more slowly. This means that Figs. 2 and 4 in Neilson et al. where the predictions are larger than the observed values are even more difficult to reconcile with the expected *mean* period changes.

The period variation in Polaris challenges the current models. In a number of stars period change is not monotonic, but rather a combination of increase and decrease (e.g., Fig. 3 in Berdnikov et al. 1997). The simplest explanation for Polaris and other overtone pulsators would be that the current epoch reflects, at least partly, short term unsteadiness rather than long term evolution. Some possible scenarios where pulsation might influence the perceived period change in overtone pulsators are sketched in Evans et al. (2002).

That said, Polaris does have an unusually large period change.

4.2.5. Which Instability Strip Crossing?

Neilson (2014) provides a recent thorough discussion of the observations of Polaris, together with evolutionary models, mass loss, rotation, and abundance. A question related to the period change is the crossing of the instability strip. T13 have asserted that their distance is consistent with a first crossing. This, however, has been refuted by van Leeuwen (2013) and Neilson (2014) and is not consistent with our mass summary above (Table 3). Following our “working model” above that period changes in overtone pulsators are not entirely due to simple monotonic evolution removes rapid period change as an argument for Polaris as a star on the first crossing of the instability strip.

Anderson (2018) has recently proposed a different interpretation for Polaris, that it is in the first crossing of the instability strip and pulsating in the first overtone. This is based in the comparison of the the luminosity of B18 with evolutionary tracks from the Geneva group (Anderson et al. 2014), as well as CNO abundance enhancements (discussed below). A major implication of this interpretation is that the mass of the Cepheid is $7 M_{\odot}$. However, mass of Polaris based on the new *Gaia* distance ($3.45 \pm 0.75 M_{\odot}$; Table 3) is inconsistent with this.

Thus, based on the period and luminosity, Polaris is on the third crossing of the instability strip.

4.2.6. Mass Loss

Could the current mass of Polaris have been affected by mass loss? The question of whether Cepheids lose mass, and in particular whether pulsation fosters mass loss is an important one. This has been a suggestion to solve the “Cepheid mass problem”, reconciling the larger evolutionary track masses with smaller pulsation predictions. Neilson et al. (2012) and references therein discuss studies which indicate that pulsation can drive mass loss. They conclude that mass loss is necessary to explain period change predictions (but we argue above for complexities in the interpretation of the period change). Observationally, there have been a series of interferometric observations indicating circumstellar envelopes (CSEs) in the K -band (Kervella et al. 2006; Mérand et al. 2006, 2007). This feature seems to be shared by all the Cepheids observed, but not the nonvariable yellow supergiant α Per. These shells are particularly important to characterize and understand since they are dependent both on wavelength and pulsation period. Thus they could affect the infrared (IR) Leavitt (period-luminosity) law and may indicate mass loss. On the other hand, *Spitzer* observations have found only occasional indications of extended IR emission (Barmby et al. 2011). Specifically, 10% have fairly clear emission, with a further 14% with tentative emission. This agrees with the summary of mid-infrared excess by Schmidt (2015). He finds that only 9% of classical Cepheids have IR excess (omitting 3 with anomalous energy distributions) and only stars with periods 11^d or longer. Thus, while there is evidence that a small fraction of Cepheids have extended IR emission, it is by no means universal. Uniquely in the case of δ Cep there is also a more extended feature in the *Spitzer* study which looks like a bow shock (Marengo et al. 2010). This was followed up by Matthews et al. (2012) with a H I 21 cm observation consistent with an outflow.

For Polaris itself, a CSE has been detected (Mérand et al. 2006). However, *Spitzer* IRAC and MIPS observations have found only a suggestion of IR excess in Polaris (Marengo

et al. 2010) and no extended IR emission (Barnby et al. 2011).

Recent X-ray observations have revealed another process which may contribute to upper atmosphere mass motions. The passage of the pulsation wave at minimum radius through the photosphere and chromosphere is marked disturbances such ultraviolet emission lines, most clearly shown in δ Cep itself (Engle et al. 2017). X-rays, on the other hand remain low and constant at minimum radius, but exhibit a sharp rise and fall just after maximum radius. One possible mechanism for this is a flare such as frequently found on the sun and other stars with convective surfaces. Often flares are associated with coronal mass ejections. The burst of X-rays in Cepheids appears to be tied to the pulsation cycle, above the photosphere, and triggered by the collapse of the atmosphere after maximum radius. Thus it is possible that the X-ray bursts may be part of a chain that moves material upward in Cepheid atmospheres.

Polaris is a very low-amplitude Cepheid, and as yet an X-ray burst has not been detected (Evans et al. 2018). However, the phase range where it would be expected has not been fully covered by X-ray observations.

4.2.7. Mergers

Figure 9 shows the positions of V1334 Cyg and Polaris Aa and B in the color-magnitude diagram (CMD; reddening-corrected absolute V magnitude versus $B - V$ color). B18 pointed out that Polaris B lies above the main sequence in the CMD, if the relatively small parallax that they found is assumed. This remains true even if we use the larger *Gaia* parallax, as shown in Figure 9. Also plotted are MIST isochrones for solar metallicity and zero rotation, for ages of 100 Myr and 2.25 Gyr. The nominal 100 Myr isochrone fits the locations of the two Cepheids reasonably well. The 2.25 Gyr isochrone was chosen

because it fits the position of Polaris B. We have argued in Section 4.2.3 that evolutionary tracks for the “blue loop” phase require some adjustment, specifically that the observed masses of the two Cepheids are significantly smaller than predicted by the luminosity of the isochrones. However, the 100 Myr isochrone in Figure 9 provides a schematic description of the evolution of a Cepheid which is clearly a reasonably massive evolved star with an age of order 100 Myr.

The apparent discordance between the ages of Polaris and its wide companion was discussed by B18. Setting aside the remote possibility that B is not actually a physical companion of the Cepheid, B18 considered two scenarios: (1) The Polaris system is young, and the B component is abnormally luminous. This could conceivably be due to B being an unresolved binary, even at *HST* resolution, although there is no direct evidence for this. We are currently planning an observation with the CHARA array to test whether B can be resolved. This might, of course, affect the *Gaia* parallax. Or possibly B is temporarily over-luminous due to a recent stellar merger. (2) Alternatively, the system may in fact be old, and it is Polaris itself that appears anomalously young. For example, Polaris might be a merger product. It certainly seems likely that at least some Cepheids are descendants of merged binaries, given the high frequency of close binaries among their B-type progenitors. In fact, Neilson et al. (2015) have pointed out an age discrepancy for the binary eclipsing LMC Cepheid OGLE-LMC-CEP1812, and presented arguments that this Cepheid is a post-merger product. Based on the MIST 2.25 Gyr isochrone, the mass of Polaris B is $\sim 1.4 M_{\odot}$, and stars of $\sim 1.6 M_{\odot}$ have essentially completed their evolution. Since we find a dynamical mass for Polaris Aa of $3.45 \pm 0.75 M_{\odot}$, a merger scenario based on two stars both near the main-sequence turnoff at $\sim 1.5 M_{\odot}$ appears possible.

We investigated whether Polaris Ab provides any useful constraint on these two scenarios. For example, if Ab also appeared to be an old star, that would greatly strengthen

the merger scenario for the Cepheid progenitor. Unfortunately, other than the dynamical mass of $1.63 \pm 0.49 M_{\odot}$, the only information we have on the nature of Polaris Ab is its absolute magnitude in the F220W (2200 Å) bandpass, which we measure in our ACS/HRC frames to be about +4.25 (Vega scale, *Gaia* distance). We have no direct information on its color or spectral type. The MIST isochrones provide absolute magnitudes in the F220W bandpass, but such an absolute magnitude can be attained by a star of this mass with either the young or old isochrones plotted in Figure 9.

4.2.8. Abundances

Abundances provide clues to the history of an evolved star. Specifically, an increase in N and a decrease in C compared with main sequence values indicates processed material. The abundances of Polaris have been measured several times, summarized by Usenko et al. (2005), including Luck & Bond (1986). Similarly, abundances for V1334 Cyg have been measured by Takeda et al. (2013). Abundances from Usenko et al. and Takeda et al. are summarized in Table 4, showing very similar amounts N enrichment and C decrease suggesting comparable processing mechanisms and quantity. As discussed by Neilson (2014), the processing of material could come either through rotational mixing near the main sequence or dredge-up as a star becomes a red giant. He computes evolutionary tracks with a range of main sequence rotational velocities. From these predictions and the relatively low observed rotational velocity he concludes that rotational mixing is not responsible for the abundance distribution hence the star must be beyond the first crossing of the instability strip. Anderson (2018) on the other hand comes to the opposite conclusion from the abundances, that they are consistent with a first crossing. We note that Figs. 8, 10, and 11 in Anderson et al. (2014) show that the N and C abundances are roughly in agreement with either pre-dredge-up with a lot of initial rotation or post-dredge-up with

little initial rotation. Takeda et al. surveyed 12 Cepheids at several phases in the pulsation cycle for each. The C and N abundances (in the mean) also agree with those of V1334 Cyg and Polaris, providing no evidence for an evolutionary state other than the post-dredge-up state typical of Cepheids.

A further mechanism which would produce processed material is the merger of a close main sequence binary (previous section).

4.3. Future Work

These results conclude the work possible with *HST* in resolving Polaris Aa and Ab since the separation between the two stars becomes progressively smaller during the following years. In this discussion we are providing a summary of the understanding of the system at present. Clearly continued study of the orbit over the next few years will provide an improved definition of the orbit and the mass. These observations are to be continued with the interferometry (e.g., the CHARA array). In fact a tentative detection has been made, which is in reasonable agreement with the current orbit.

5. Summary

To summarize, Polaris now has a suite of directly measured parameters to identify its physical state: luminosity, mass, radius, period change, and abundance, although we stress that the mass presented here is preliminary, and Tables 2 and 3 illustrate the dependence on the data string and the distance. The mass is within approximately 1σ of the mass of V1334 Cyg, which is more precisely measured. However, for both Polaris and V1334 Cyg, the masses are smaller than predicted by evolutionary tracks for the observed luminosities. There are several suggestions of the more complex history for Polaris in arriving at its

present configuration. It has a circumstellar envelope in the infrared, making it likely that some mass has been lost. The interpretation of the rapid period change is likely to involve more than evolution through the instability strip alone, but also may be characteristic of overtone pulsation. In agreement with this is the fact that V1334 Cyg (also an overtone pulsator) has no measurable period change. The difference in age required for isochrones for Polaris Aa and B suggests that the Cepheid might be a merger product. Probing these questions is the goal of further observations of the orbit.

It is a pleasure to thank Pierre Kervella for valuable comments on the draft. Support for this work was provided by NASA through grants from the Space Telescope Science Institute (HST-GO-10891.01-A and HST-GO-13369.001-A), which is operated by the Association of Universities for Research in Astronomy, Incorporated, under NASA contract NAS5-26555. Support for this work was also provided from the Chandra X-ray Center NASA Contract NAS8-03060. G.H.S. acknowledges support from NSF Grant AST-1411654. VizieR and SIMBAD were used in the preparation of this study. This work has made use of data from the European Space Agency (ESA) mission *Gaia* (<https://www.cosmos.esa.int/gaia>), processed by the *Gaia* Data Processing and Analysis Consortium (DPAC, <https://www.cosmos.esa.int/web/gaia/dpac/consortium>). Funding for the DPAC has been provided by national institutions, in particular the institutions participating in the *Gaia* Multilateral Agreement.

REFERENCES

- Anderson, R. I. 2018, arXiv 1803:07413
- Anderson, R. I., Ekstrom, S., Georgy, C., Meynet, G., Mowlavi, N., & Eyer, L. 2014, A&A564, 100
- Anderson, R. I., Saio, H., Ekstrom, S., Georgy, C., & Meynet, G. 2016, A&A591, 8
- Barmby, P., Marengo, M., Evans, N.R., Bono, G., Huelsman, D., Su, K.Y.L., Welch, D. L., & Fazio, G.G. 2011, AJ, 141, 42
- Benedict, G. F., McArthur, B. E., Feast, M. W. et al. 2007, AJ, 133, 1810
- Berdnikov, L. N., Ignatova, V. V., Pastukhova, E. N., & Turner, D. G. 1997, AstL, 23, 177
- Bond, H. E., Nelan, E. P., Evans, N. R., Schaefer, G. H., & Harmer, D. 2018, ApJ, 853, 55 (B18)
- Bono, G., Gieren, W. P., Marconi, M., Fouqué, P., Caputo, F. 2001, ApJ, 563, 319
- Bressan, A., Marigo, P., Girardi, L., et al. 2012, MNRAS, 427, 127
- Bruntt, H., Evans, N. R., Stello, D. et al. 2008, ApJ, 683, 433
- Choi, J., Dotter, A., Conroy, C., Cantillo, M., Paxton, B., and Johnson, B. D. 2016, ApJ, 823, 102
- Engle, S. G., Guinan, E. F., Harper, G. M., Cuntz, M., Evans, N. R., Neilson, H., & Fawzy, D. E. 2017, ApJ, 838, 67
- Esch, D. N., Connors, A., Karovska, M., & van Dyk, D. A. 2004, ApJ, 610, 1213
- Evans, N. R. 1988, PASP, 100, 724

- Evans, N. 2000, AJ, 119, 3050
- Evans, N. R., Bond, H. E., Schaefer, G. H. et al. 2013 AJ 146, 93
- Evans, N. R., Engle, S., Guinan, E., Neilson, H., Marengo, M., Matthews, L., & Günther, H. M. 2018, Proc. RR Lyr 2017 Conf.
- Evans, N. R., Sasselov, D. D., & Short, C. I. 2002, ApJ, 567, 1121
- Evans, N. R., Schaefer, G. H., Bond, H. E., et al. 2008, AJ, 136, 1137 (E08)
- Evans, N. R., Szabo, R., Derekas, A., et al. 2015, MNRAS, 446, 4008
- Evans, N. R., & Teays, T. J. 1996, AJ, 112, 761
- Feast, M. W., & Catchpole, R. M. 1997, MNRAS, 286, L1
- Fernie, J.D., Beattie, B., Evans, N.R., and Seager, S. 1995, IBVS No. 4148
- Gaia Collaboration, T. Prusti, J.H.J. de Bruijne, A. Brown et al. 2016 A&A 595, A1
- Gaia Collaboration, Brown, A. G. A., Vallenari, A., et al. 2018a, arXiv:1804.09365
- Gaia Collaboration, G. Clementini, L. Eyer, V. Ripepi et al. 2018b, A&A 605, A79
- Gallenne, A., Monnier, J. D., Mérand, A., et al. 2013, A&A, 552, A21
- Gallenne, A. Kervella, Evans, N. et al. 2018 submitted, Science
- Gallenne, A., Mérand, A., Kervella, P., et al. 2015, A&A 579, 68
- Georgy, C., Ekstrom, S., Granada, A., Meynet, G., Mowlavi, N., Eggenberger, P. and Maeder, A. 2013, A&A, 553, 24
- Kamper, K. W. 1996, JRASC, 90, 140 (K96)

- Karovska, M., Schlegel, E., Hack, W., Raymond, J. C., & Wood, B. E. 2005, *ApJ*, 623, L137
- Karovska, M., Gaetz, T.J., Carilli, C.L., Hack, W., Raymond, J. C., & Lee, N.P., 2010, *ApJ Let.*, 710, 132
- Kervella, P., Mérand, A., Perrin, G., & Coude du Foresto, V. 2006, *A&A*, 448, 623
- Kervella, P., Bond, H. E., Cracraft, M., et al. 2014, *A&Ap*, 572, A7
- Lindgren, L., Hernandez, J., Bombrun, A. et al. 2018 arXiv:1804.09366
- Luck, R. E., & Bond, H. E. 1986, *PASP*, 98, 442
- Lucy, L. B. 1974, *AJ*, 79, 745
- Marengo, M., Evans, N.R., Barmby, P., et al. 2010, *ApJ*, 725, 2392
- Matthews, L. D., Marengo, M., Evans, N. R., & Bono, G. 2012, *ApJ*, 744, 53
- Mérand, A., Aufdenberg, J. P., Kervella, P. et al. 2007, *ApJ*, 664, 1093
- Mérand, A., Kervella, P., Coude du Foresto, V. 2006, *A&A*, 453, 155
- Neilson, H. R. 2014, *A&A*, 563, 48
- Neilson, H. R., Langer, N., Engle, S. G., Guinan, E., & Izzard, R. 2012a, *ApJ*, 760, L18
- Neilson, H. R., Engle, S. G., Guinan, E., Langer, N., Wasatonic, R. P., and Williams, D. B. 2012b, *ApJ*, 745, L32
- Neilson, H. R., Izzard, R. G., Langer, N., & Ignace, R. 2015, *A&A*, 581, L1
- Pilecki, B., Gieren, W., Pietrzynski, G. et al. 2018 arXiv 1806:01391
- Poretti, E., Le Borgne, J.F., Rainer, M., et al. 2015, *MNRAS*, 454, 849

- Richardson, W. H. 1972, *J. Opt. Soc. Am.*, 62, 1, 55
- Riess, A. G., Casertano, S., Yuan, W., et al. 2018a arXiv:1804.10655
- Riess, A. G., Casertano, S., Yuan, W., et al. 2018b, *ApJ*, 855, 136
- Roemer, E. 1965, *ApJ*, 141, 1415
- Sahu, K., Baggett, S., & MacKenty, J. 2014, *Space Telescope Instrument Science Report WFC3 2014-009* (Baltimore: STScI)
- Schmidt, E. G. 2015, *ApJ*, 813, 29
- Smolec, R. & Sniegowska, M. 2016, *MNRAS*, 458,3561
- Spreckley, S. A. & Stevens, I. R. 2008, *MNRAS*, 388, 1239
- Szabados, L. 1983, *Ap&SS*, 96, 185
- Szabados, L. 1977, *Mitt Sternw Ungarish Akad Wissen*, 70, 1
- Szabados, L. 1980, *Mitt Sternw Ungarish Akad Wissen*, 76, 1
- Szabados, L. 1981, *Mitt Sternw Ungarish Akad Wissen*, 77, 1
- Szabados, L. 1989, *Mitt Sternw Ungarish Akad Wissen*, 94, 1
- Szabados, L. 1991, *Mitt Sternw Ungarish Akad Wissen*, 96, 125
- Takeda, Y., Kang, D.-I., Han, I., Lee, B.-C., and Kim, K.-M. 2013, *MNRAS*, 432, 769
- Turner, D. G., Abdel-Latif, M. A., & Berdnikov, L. N. 2006, *PASP*, 118, 410
- Turner, D. G., Kovtyukh, V. V., Usenko, I. A., & Gorlova, N. I. 2013 *ApJ*, 762, L8 (T13)
- Turner, D. G., Savoy, J., Derrah, J., Abdel-Latif, M. A., & Berdnikov, L. N. 2005, *PASP*, 117, 207

Usenko, I. A., Miroshnichenko, A. S., Klochkiva, V. G., & Yushkin, M. V. 2005 MNRAS, 362, 1219

van Leeuwen, F. 2007, A&A, 474, 653 (vL07)

van Leeuwen, F. 2013, A&A, 550, L3

van Leeuwen, F., Feast, M. W., Whitelock, P. A., & Laney, C. D. 2007, MNRAS, 379, 723

Wielen, R., Jahreiss, H., Dettbarn, C., Lenhardt, H., & Schwan, H. 2000, A&A, 360, 399

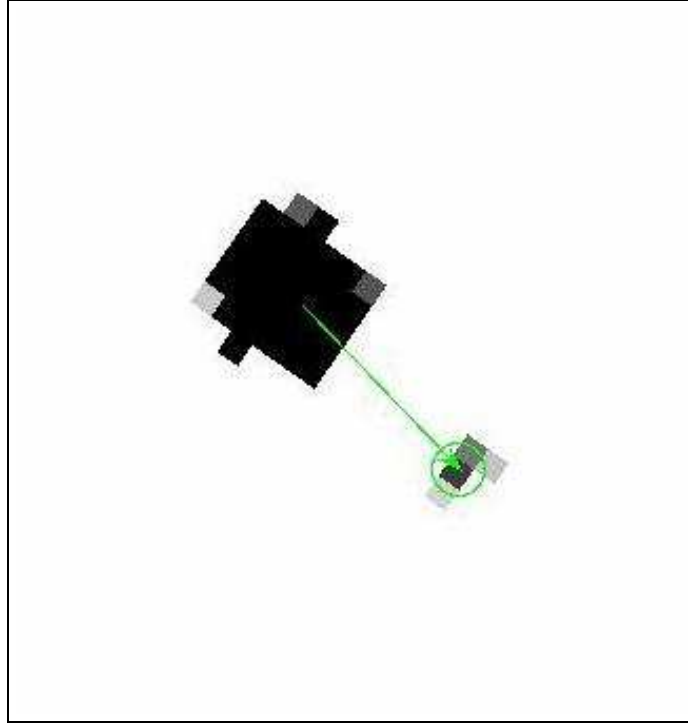


Fig. 1.— The 2007 WFPC2 image of Polaris, AstroDrizzled to a scale of $0''.02 \text{ pixel}^{-1}$, and deconvolved using an image of Polaris B as the PSF reference. The faint companion Polaris Ab is detected at a separation of $0''.18$. The green circle marking the companion has a radius of $0''.02$ and the green arrow indicates the separation of Polaris Ab from the center of the Cepheid Polaris Aa. In Figures 1 through 3, north is at the top and east at the left.

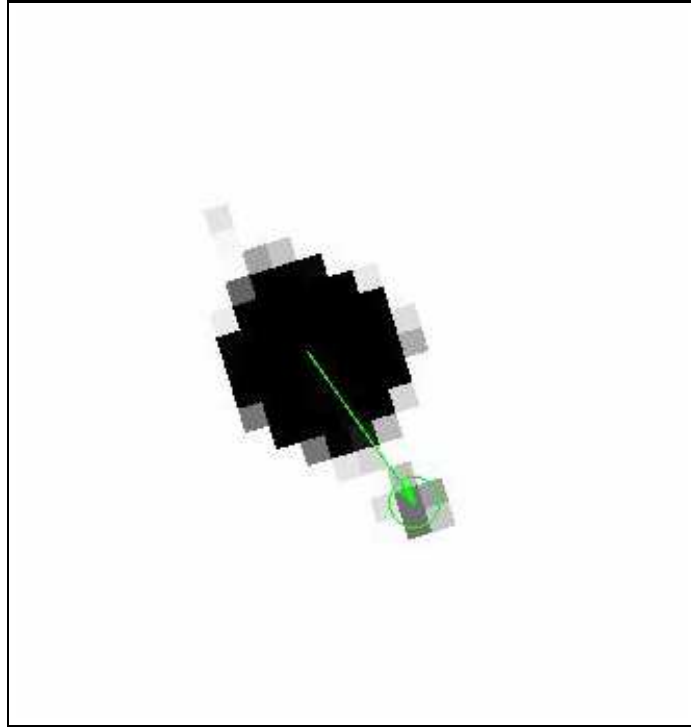


Fig. 2.— The 2009 WFC3 image of Polaris, AstroDrizzled to a scale of $0''.02 \text{ pixel}^{-1}$, and again deconvolved using an image of Polaris B as the PSF reference. The companion is detected at a separation of $0''.15$. The green circle marking the companion again has a radius of $0''.02$ and the green arrow indicates the separation of Polaris Ab from Polaris Aa. Note slight elongation of the image due to “shutter jitter” in the short WFC3 exposures.

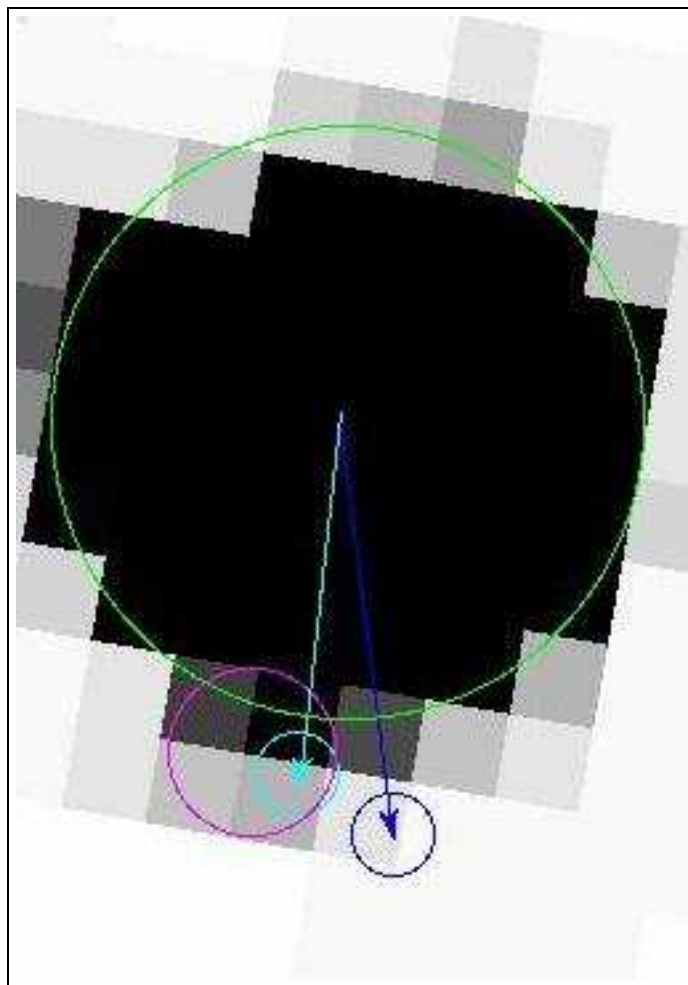


Fig. 3.— The 2014 WFC3 image of Polaris, AstroDrizzled to a scale of $0''.02 \text{ pixel}^{-1}$. This image has been deconvolved using the EMC2 algorithm (see text), with images of γ Cyg serving as the PSF reference. Note the magnified scale of this image compared to Figures 1 and 2. Here the large green circle is to guide the eye to show the location of the Cepheid. The magenta circle is where we believe we have detected the companion, lying $0''.08$ from the Cepheid. The dark blue circle and arrow are the predicted location based on a combination of the spectroscopic orbit, our *HST* observations from 2005 to 2007, and the astrometric measurements from Wielen et al. (2000). This location is clearly offset from the brightest pixels in the area where the companion is detected. The light blue circle and orbit are the predictions from the same data varying the inclination by 1σ .

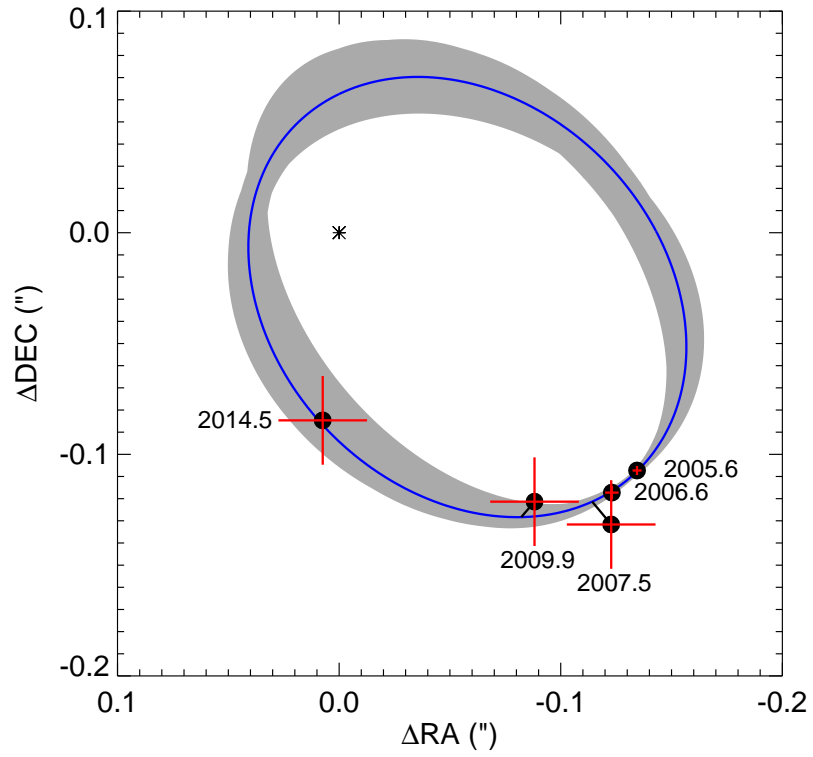


Fig. 4.— Visual orbit of Polaris Ab relative to Aa, based on our *HST* measurements. Black circles show the measured positions. The sizes and orientations of the error ellipses are shown as red lines. The blue curve shows the best-fit orbit, determined as described in the text. The shaded gray area shows the range of orbital solutions that fit the data.

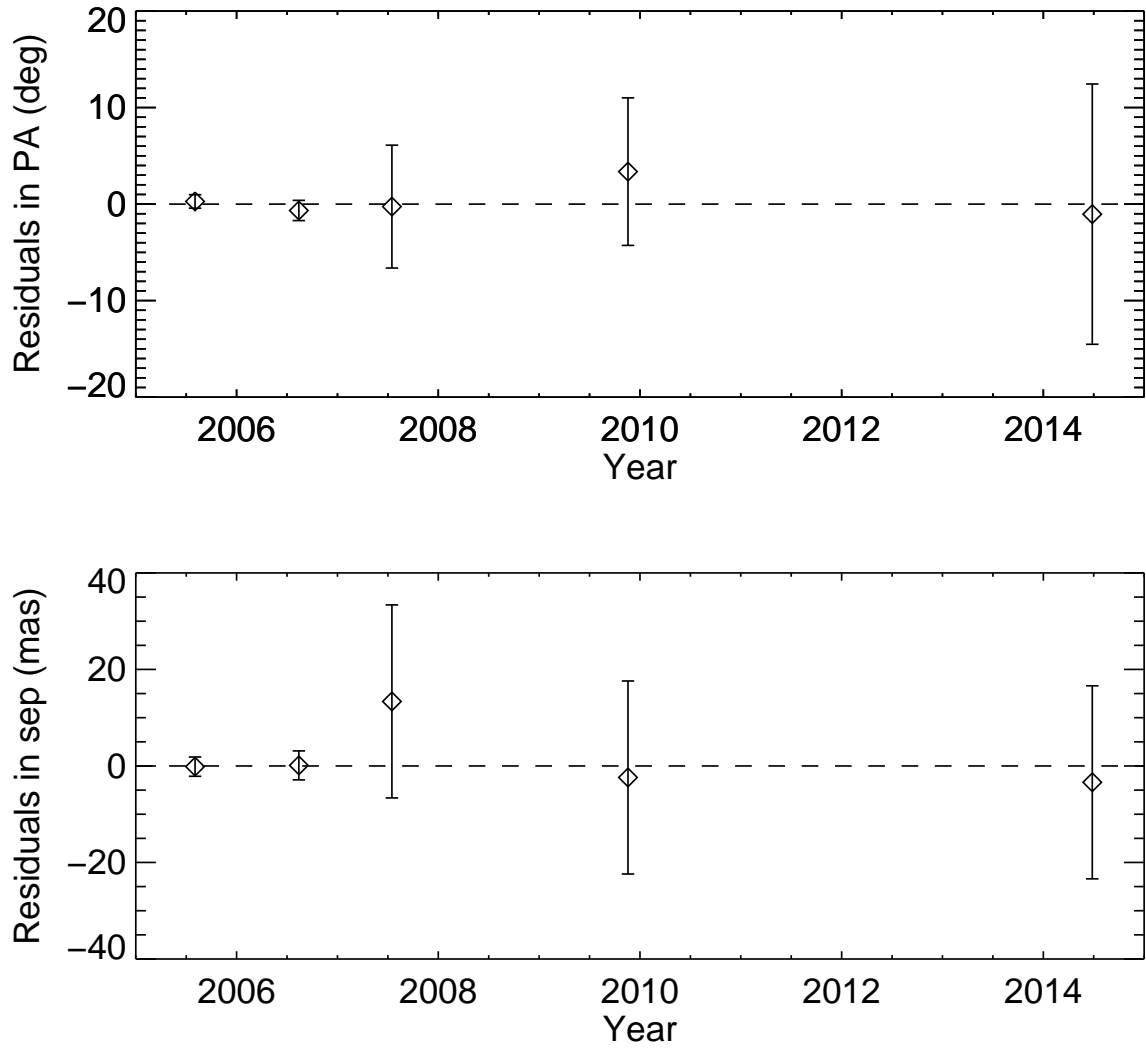


Fig. 5.— Residuals in the position angle and separation measured with *HST* and the best-fit orbital solution.

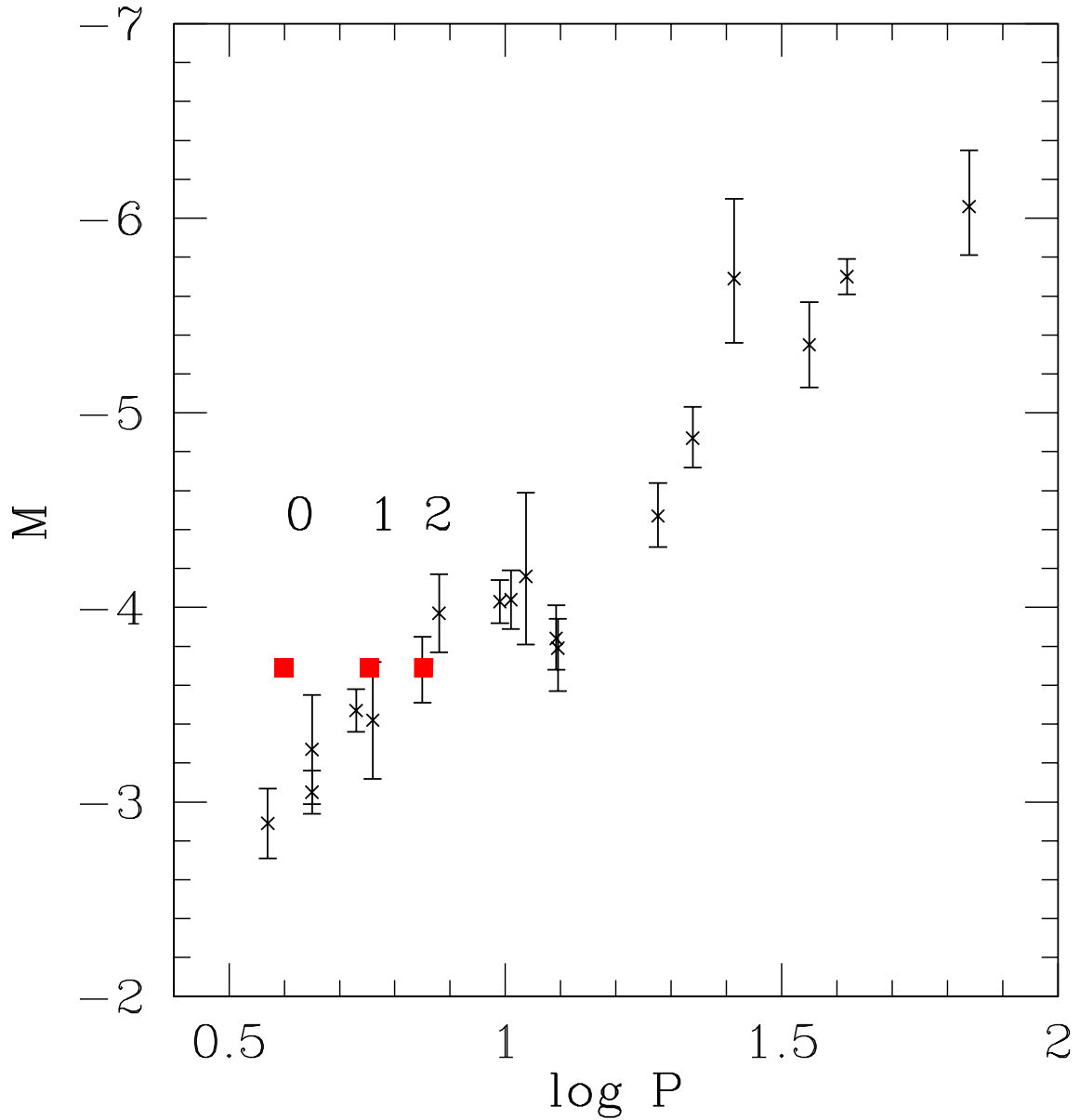


Fig. 6.— Polaris in the context of the Leavitt Law. Polaris M_V from *Gaia*: filled red squares; other Cepheids: x’s from FGS, *HST* spatial scans, and RS Pup (see text). The labels above the values for Polaris indicate the pulsation period adjusted (left to right) to the fundamental period for a star pulsating in the fundamental mode, the first overtone, and the second overtone. Note that the errors on the squares are smaller than the symbols (including one overlapping an x giving the appearance of a large error). M_V is in magnitudes; P is in days.

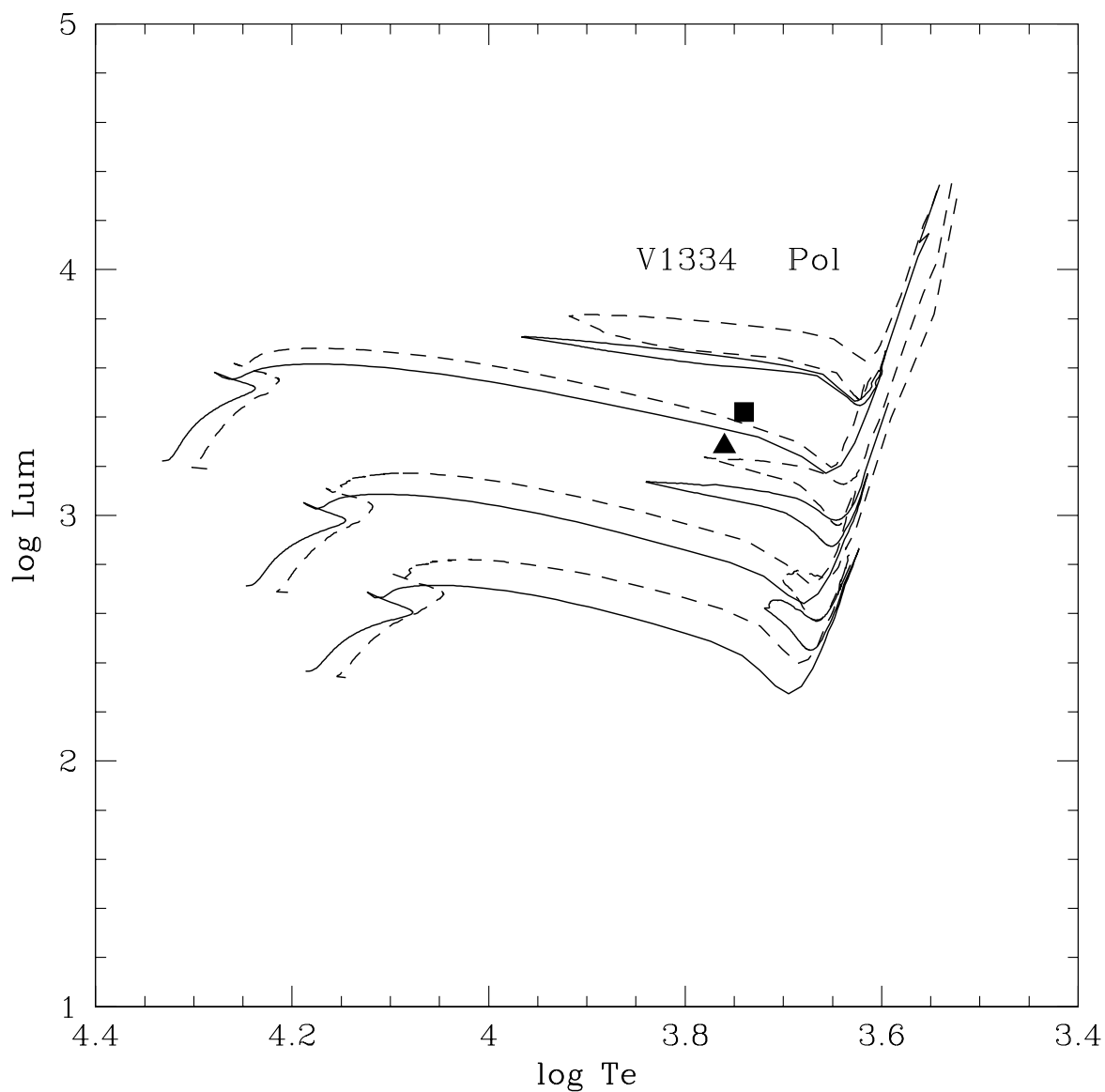


Fig. 7.— Polaris and V1334 Cyg compared with evolutionary tracks. For Polaris (filled square) and V1334 Cyg (filled triangle) the errors are error smaller than the symbols. The relative positions of Polaris and V1334 Cyg are shown by the labels. The evolutionary tracks from Georgy et al. (2013) are 4, 5, and 7 M_\odot from bottom to top. Solid lines are for 0 rotational velocity on the main sequence; dashed lines have 0.95 breakup velocity. Luminosity is in solar units; temperature is in K.

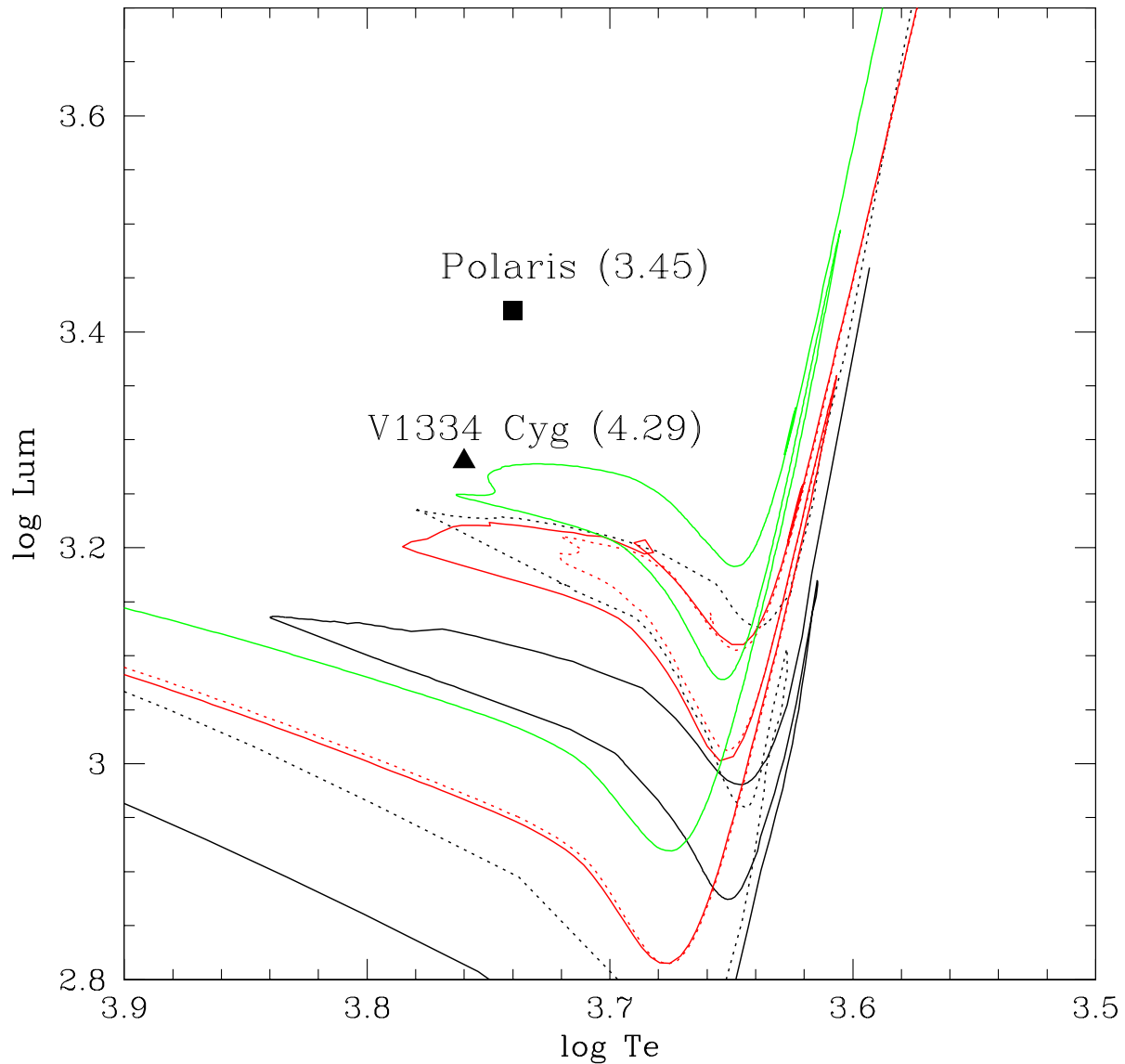


Fig. 8.— Polaris and V1334 Cyg compared with evolutionary tracks in the region of the “blue loops”. For Polaris (filled square) and V1334 Cyg (filled triangle) the errors are smaller than the symbols. The mass in M_{\odot} is listed next to the star name. The evolutionary tracks from Georgy et al. (2013): black; MIST: red; and PARSEC (green), all for $5 M_{\odot}$. Solid and dotted lines represent no rotation and significant rotation respectively (see text). Luminosity is in solar units; temperature is in K.

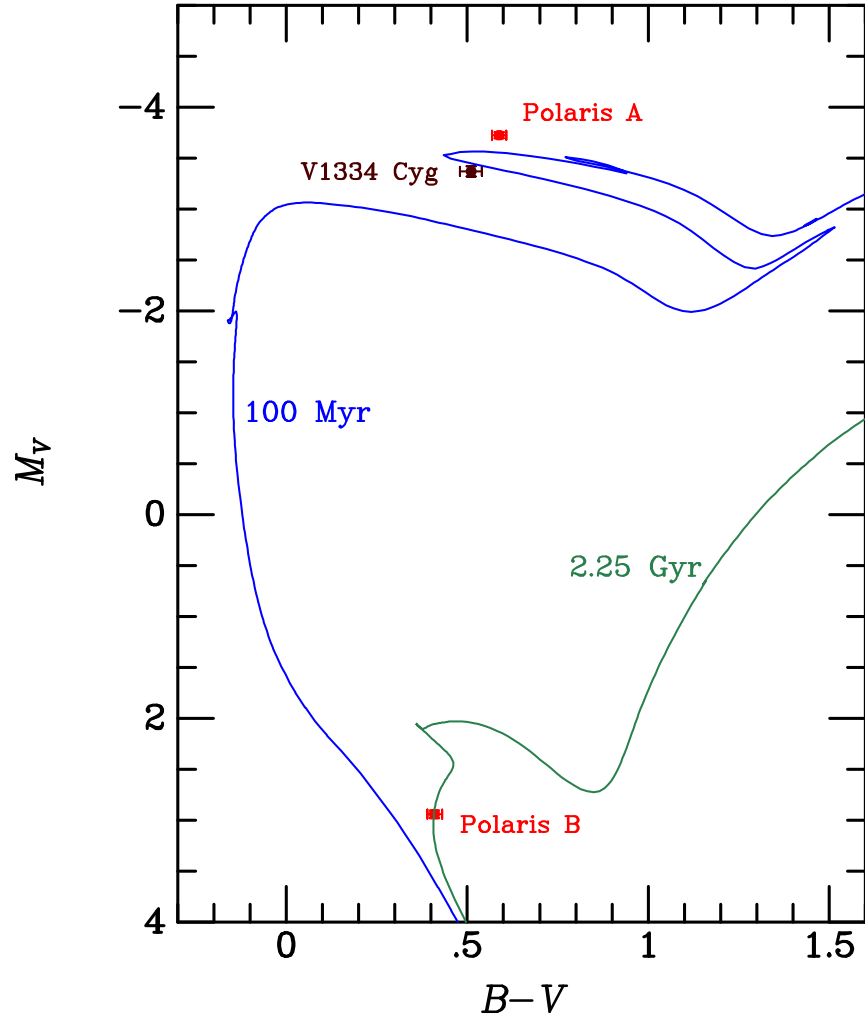


Fig. 9.— Locations in the color-magnitude diagram (absolute V magnitude vs. $B-V$ color) of the Cepheid V1334 Cyg (purple point) and Polaris Aa and B (red points). Also shown are solar-metallicity and zero-rotation isochrones from the MIST data base (see text) for ages of 100 Myr (blue line) and 2.25 Gyr (green line).

Table 1. *HST* Imaging Observations and Measurements of Polaris Aa–Ab

UT Date	Besselian Date	Program ID ^a	Instrument	Filter	P.A. (J2000) ^b [degrees]	Separation [arcsec]
2005 Aug 2–3 ^c	2005.5880	GO-10593	ACS/HRC	F220W	231.4 ± 0.7	0.172 ± 0.002
2006 Aug 13 ^c	2006.6172	GO-10891	ACS/HRC	F220W	226.4 ± 1.0	0.170 ± 0.003
2007 Jul 17 ^d	2007.5402	GO-11293	WFPC2/PC	F218W	223 ± 6.4	0.18 ± 0.02
2009 Nov 18 ^d	2009.8813	GO-11783	WFC3/UVIS	FQ232N	216 ± 7.6	0.15 ± 0.02
2014 Jun 26 ^e	2014.4856	GO-13369	WFC3/UVIS	FQ232N	175 ± 13.5	0.085 ± 0.02

^aN.R.E. was Principal Investigator for all of these programs.

^bNote that the P.A. is referred to the J2000 equator, not to the equator of the observation epoch as is the usual custom in ground-based visual-binary work.

^cInformation for the first two observations is quoted from Evans et al. 2008.

^dIn 2007 and 2009 we also obtained images of Polaris B, for use as a PSF reference.

^eWFC3 observations were also obtained on 2014 Mar 17, but were not used in the analysis (see text). The 2014 observations were accompanied by a set of nearly identical exposures on γ Cyg for PSF reference purposes.

Table 2. Orbital Parameters for Polaris Aa–Ab

Parameter	Value (All data)	Value (Omitting 2014)	Reference
P [yr]	29.59 ± 0.02	29.59 ± 0.02	Kamper (1996)
T_0	1987.66 ± 0.13	1987.66 ± 0.13	Wielen et al. (2000)
e	0.608 ± 0.005	0.608 ± 0.005	Kamper (1996)
ω_{Aa} [$^\circ$] ^a	303.01 ± 0.75	303.01 ± 0.75	Kamper (1996)
a [$''$]	0.1204 ± 0.0059	0.1215 ± 0.0062	This work
i [$^\circ$]	146.2 ± 10.9	144.1 ± 10.0	This work
Ω [$^\circ$] ^b	191.4 ± 4.9	192.1 ± 4.7	This work
χ^2_ν	0.179	0.241	This work

^aThe angle between the ascending node and periastron passage, as referenced to Polaris Ab is given by $\omega_{Ab} = \omega_{Aa} + 180^\circ = 123.01^\circ$.

^b Ω is flipped by 180 deg compared with the value reported in Table 4 of Evans et al. (2008) because the earlier paper defined $\omega_{Ab} = 303.01$ deg in the visual orbit fit, rather than using the standard spectroscopic convention of referencing ω to the primary.

Table 3. Dynamical Masses for Polaris Aa and Ab for Different Adopted Parallaxes

Parameter	— Parallax adopted from: ^a —	
	vL07	G18
π [mas]	7.54 ± 0.11	7.3218 ± 0.0281
d [pc]	132.6 ± 1.9	136.58 ± 0.52
M_{tot} [M_{\odot}]	4.65 ± 0.71	5.07 ± 0.75
M_{Aa} [M_{\odot}]	3.11 ± 0.70	3.45 ± 0.75
M_{Ab} [M_{\odot}]	1.54 ± 0.46	1.63 ± 0.49
$\langle M_{V,\text{Aa}} \rangle^{\text{b}}$	-3.66 ± 0.04	-3.73 ± 0.03

^aAbbreviations for sources of adopted parallaxes are vL07 = van Leeuwen 2007; G18 = *Gaia* including Lindegren correction.

^bMean visual absolute magnitude of Polaris Aa, assuming $\langle V \rangle = 1.982$, $E(B - V) = 0.01 \pm 0.01$, and the adopted parallax.

Table 4. Abundances

	[C/H]	[N/H]	[O/H]
Polaris Aa	-0.17	+0.42	-0.00
V1334 Cyg	-0.24 ± 0.03	$+0.44 \pm 0.03$	$+0.03 \pm 0.03$